

Three-Dimensional Adaptive Filtering in Magnetic Resonance Angiography

Carl-Fredrik Westin, PhD,^{1*} Lars Wigström, MSc,^{2,3} Tomas Loock, MSc,⁴
Lars Sjöqvist, PhD,⁴ Ron Kikinis, MD,¹ and Hans Knutsson, PhD³

In order to enhance 3D image data from magnetic resonance angiography (MRA), a novel method based on the theory of multidimensional adaptive filtering has been developed. The purpose of the technique is to suppress image noise while enhancing important structures. The method is based on local structure estimation using six 3D orientation selective filters, followed by an adaptive filtering step controlled by the local structure information. The complete filtering procedure requires approximately 3 minutes of computational time on a standard workstation for a $256 \times 256 \times 64$ data set. The method has been evaluated using a mathematical vessel model and in vivo MRA data (both phase contrast and time of flight (TOF)). 3D adaptive filtering results in a better delineation of small blood vessels and efficiently reduces the high-frequency noise. Depending on the data acquisition and the original data type, contrast-to-noise ratio (CNR) improvements of up to 179% (8.9 dB) were observed. 3D adaptive filtering may provide an alternative to prolonging the scan time or using contrast agents in MRA when the CNR is low. *J. Magn. Reson. Imaging* 2001;14:63-71. © 2001 Wiley-Liss, Inc.

Index terms: angiography; adaptive filtering; noise reduction; tensor; image enhancement

MOST MAGNETIC RESONANCE ANGIOGRAPHY (MRA) techniques produce a 3D data set, which is processed to selectively display the vasculature of interest. Angiograms based on both phase contrast (1) and time of flight (TOF) (2) can be reconstructed from the 3D data sets using maximum intensity projection (MIP), which creates a 2D image by recording the intensity of the brightest voxel along each projection ray through the

3D volume (3). The MIP technique is sensitive to high-intensity values that tend to obscure regions of slow or recirculating flow, is unable to separately identify arterial and venous structures within the same data, and cannot discriminate high-intensity artifacts from true vessel signal (4). A high-resolution data set acquired while maintaining a short scan time often has a noise level high enough to obscure important diagnostic information in the angiograms. Several methods for reduction of noise in MRA data have been published (5-19). Song et al. presented a method to reduce the noise in 3D phase-contrast MRA (10). The method exploits the fact that the velocity field is divergence-free. The noise contribution, which is not divergence-free, can be removed using a projection operator method in Hilbert space. Du and coworkers showed that 3D TOF images could be improved by using a nonlinear second difference spatial filtering technique (11). Comparison with a Laplacian filtering technique demonstrated that the contrast-to-noise ratio (CNR) increased when the nonlinear second difference spatial method was employed. Reducing noise without blurring the lines and edges encourages intraregion smoothing in preference to smoothing across regions. Perona and Malik developed a multiscale smoothing and edge detection scheme, mathematically formulated as an anisotropic diffusion process that effectively performed intraregion smoothing (12). This work was later extended to 3D and adapted for MR imaging (MRI) by Gerig et al. (13). More recent enhancement filters are based on diffusion derived from the affine heat equation (14,15). This formulation has been shown to yield implementations that are more numerically stable. Chen and Hale describe how to reduce noise and enhance small vessels in 3D MR angiograms using directed low-pass filters (16). Sun et al used directional filtering of digital coronary arteriograms for the quantification of percent diameter stenosis (18). Sato et al. recently presented a 3D filtering technique for curvilinear structures based on a combination of the eigenvalues of the Hessian matrix (19). They demonstrate the usefulness of the method by segmenting brain vessels from MRA, bronchi from a chest CT, and portal veins from an abdominal CT.

Multidimensional adaptive filtering is used as a technique for enhancement of images, image volumes, and volume sequences having temporal resolution, i.e., 2D

¹Surgical Planning Laboratory, Brigham and Women's Hospital and Harvard Medical School, Boston, Massachusetts.

²Department of Medicine and Care, Clinical Physiology, Linköping University, Linköping, Sweden.

³Department of Biomedical Engineering, Linköping University, Linköping, Sweden.

⁴MRI Unit, Department of Radiation Physics and Radiology, Linköping University Hospital, Linköping, Sweden.

Contract grant sponsor: Swedish Medical Science Foundation; Contract grant number: B94-39X-10885-01; Contract grant sponsor: NIH; Contract grant numbers: P41-RR13218; R01-RR11747; Contract grant sponsor: Center for Integration of Medicine and Innovative Technology (CIMIT).

*Address reprint requests to: C.-F.W., Surgical Planning Laboratory, Brigham and Women's Hospital and Harvard Medical School, 75 Francis St., Boston, MA 02115. E-mail: westin@bwh.harvard.edu

Received August 25, 2000; Accepted December 28, 2000.

to 4D data (22). The multidimensional adaptive filtering method employs the local orientation of structures within the image, such as lines, edges, and planes, to control a set of anisotropic filters. The filters are adaptive with respect to bandwidth and local orientation of the input signal. The filter design is based on the concept of using quadrature filters for orientation estimation (25). The basic idea is to reduce the noise in large, low-frequency regions and to enhance features such as lines and planes. In 3D MRA, small vessels correspond to lines and the surface of larger vessels to planes.

In this paper we present a novel application of multidimensional adaptive filtering (22). The method has been implemented to enhance 3D MRA data, acquired using both phase-contrast and TOF techniques. 3D enhancement of the cerebral vessels and the renal arteries are shown as examples. The basic principles of the theory and implementation details are presented. The method is, however, general, and the theoretical expressions are applicable to all types of 3D MRI data.

THEORY

The theory of multidimensional adaptive filtering is described and the analytical expressions for 3D filtering are derived below. A thorough treatment of the theoretical details for multidimensional, 2D to 4D, adaptive filtering has been presented previously (20–24). The method is divided into three main steps. The first step includes an estimation of the local orientation of every neighborhood in the original image by assuming that the local orientation can be described by simple features such as lines and planes. In the second step the orientation estimate is stabilized through low-pass filtering. Subsequently, the orientation information is used to control the filtering of the original data in an adaptive fashion.

Orientation Estimation

An orientation estimation algorithm is employed to obtain information about local structures (24,27–31). A suitable vector representation for orientation in 2D has been described previously (25,26). The tensor representation of orientation in 2D to 4D used in this work was first suggested by Knutsson (27–29). The algorithm detects the existence of lines and planes in every neighborhood of an image volume in 3D. Special complex filters, so-called quadrature filters, have shown to be useful for detecting edges and lines (25). A quadrature filter, $F_k(\mathbf{u})$, is given by

$$\begin{cases} F_k(\mathbf{u}) = F_{radial}(\rho)(\hat{\mathbf{u}}^T \hat{\mathbf{n}}_k)^2 & \text{if } \hat{\mathbf{u}}^T \hat{\mathbf{n}}_k > 0 \\ F_k(\mathbf{u}) = 0 & \text{otherwise} \end{cases} \quad (1)$$

where \mathbf{u} is the coordinate vector in the Fourier domain, $\hat{\mathbf{u}}$ is a unit vector directed along \mathbf{u} , $\hat{\mathbf{n}}_k$ is the direction of filter k , and $\rho = |\mathbf{u}|$. The quadrature filter is polar separable, i.e., it can be divided into a radial $F_{radial}(\rho)$ and an angular part ($\hat{\mathbf{u}}^T \hat{\mathbf{n}}_k$). A particular feature of the quadrature filter is that the filter is zero over one-half of the Fourier space following from Eq. [1]. $F_{radial}(\rho)$ is a radial band pass function with appropriate character-

istics. A suitable radial function for estimating local image structure is based on the log normal function (22):

$$F_{radial}(\rho) = e^{(4 \ln 2 / B^2) \ln^2(\rho / \rho_c)} \quad (2)$$

where B is the relative bandwidth of the filter and ρ_c is the center frequency of the filter. $B = 2$ and $\rho_c = 1.11$ have been used throughout this work.

The output from quadrature filter k is calculated as

$$Q_k(\mathbf{u}) = F_k(\mathbf{u})S(\mathbf{u}) \quad (3)$$

where $S(\mathbf{u})$ is the Fourier transform of the original data set. The quadrature filter output in the spatial domain, $q_k(\mathbf{x})$, is obtained by taking the inverse Fourier transform of $Q_k(\mathbf{u})$. It has previously been shown that the multidimensional orientation estimation is conveniently described using the tensor formalism (27). The tensor, \mathbf{T} , describing the local structure in 3D is given by

$$\mathbf{T}(\mathbf{x}) = \sum_{k=1}^6 |q_k(\mathbf{x})| \left(\mathbf{N}_k - \frac{1}{5} \mathbf{I} \right) \quad (4)$$

where \mathbf{N}_k is a tensor representing the filter direction (see Appendix A), \mathbf{I} is the identity tensor, and \mathbf{x} is the spatial coordinate. The number of quadrature filters required for orientation estimation in 3D is six (27). These filters are directed toward the vertices in a hemi-icosahedron and span one-half of the Fourier space symmetrically.

The orientation estimate of the local neighborhood is evaluated by determining the eigenvalues and eigenvectors corresponding to \mathbf{T} . For example, the largest eigenvector of \mathbf{T} corresponds to the normal vector of the plane best describing the local neighborhood.

Stabilization of the Control Information

The orientation estimates may vary considerably in complex neighborhoods. These variations are due to the presence of mixed types of structures within the local neighborhood. This implies a disturbance of the orientation tensor and consequently the adaptive filtering. Due to the representation of local orientation, a low-pass filtering of the orientation tensors can be used to reduce the variations of the orientation estimates.

A stabilized orientation tensor field is attained by employing an isotropic Gaussian low-pass filter (22). This type of averaging will not affect the high-frequency content of the neighborhood. The stabilized orientation tensor is calculated as

$$T_{LP}(\mathbf{u}) = G_{LP}(\mathbf{u})T(\mathbf{u}) \quad (5)$$

where $G_{LP}(\mathbf{u})$ is the Gaussian low-pass filter and $T(\mathbf{u})$ is the Fourier transform of the estimated orientation tensor $\mathbf{T}(\mathbf{x})$. The purpose of the low-pass filtering is to suppress rapid spatial changes in the description of local structure.

Multidimensional Adaptive Filtering

The adaptive filtering algorithm is in the spatial domain schematically given by

$$s_{\text{adaptive}}(\mathbf{x}) = s_{\text{LP}}(\mathbf{x}) + \alpha(\mathbf{x})s_{\text{HP}}(\mathbf{x}) \quad (6)$$

where s_{HP} is a combination of the outputs from six high-pass filters F_{HP_k} ,

$$s_{\text{HP}}(\mathbf{x}) = \sum_{k=1}^6 \beta_k(\mathbf{x})s_{\text{HP}_k}(\mathbf{x}) \quad (7)$$

and s_{LP} denotes the result from applying the low-pass filter F_{LP} on the input image. s_{HP} is the corresponding high-pass filtered image, which is a combination of the results from six spatially directed filters. The contribution from each high-pass filter is controlled by β_k , so that the resulting filtering can be either isotropic or possess a varying degree of anisotropy. The parameters α and β_k are determined from T_{LP} so that low-pass filtering is performed in regions where no apparent structure is found, and high-pass filtering is performed perpendicular to structures in the input image.

The low-pass filter can be expressed as (20):

$$F_{\text{LP}}(\mathbf{u}) = \begin{cases} \cos^2\left(\frac{\pi|\mathbf{u}|}{1.8}\right) & |\mathbf{u}| \leq 0.9 \\ 0 & \text{otherwise} \end{cases} \quad (8)$$

The radial part of the high-pass filters is defined by the following function

$$F_{\text{HP}}(\mathbf{u}) = 1 - F_{\text{LP}}(\mathbf{u}) \quad (9)$$

to ensure that the signal can be fully reconstructed in noise-free regions ($F_{\text{LP}} + F_{\text{HP}} = 1$). Similar to the local structure estimation procedure (Eq. [4]), six directed filters are applied to the image in order to describe the high-frequency content in different directions. These are defined as

$$F_{\text{HP}_k}(\mathbf{u}) = F_{\text{HP}}(\mathbf{u})(\hat{\mathbf{u}}^T \hat{\mathbf{n}}_k)^2 \quad (10)$$

where $\hat{\mathbf{n}}_k$ denotes the different filter directions (see appendix A). These filters are depicted in Figure 1b–g.

Based on the stabilized orientation estimate, the filter outputs from the low-pass filter and the six high-pass filters can now be combined. This can be seen either as a combination of the filter outputs as described in Eq. [6] or as a combination of the filters to produce a new filter, which is dependent on the structures in the neighborhood where it is applied:

$$f_{\text{adaptive}}(\mathbf{x}) = f_{\text{LP}} + \alpha(\mathbf{x}) \sum_{k=1}^6 \beta_k(\mathbf{x})f_{\text{HP}_k} \quad (11)$$

where the control parameters are defined by

$$\alpha(\mathbf{x}) = h(\|T_{\text{LP}}(\mathbf{x})\|/\|T_{\text{LP}}(\mathbf{x})\|_{\text{Max}})$$

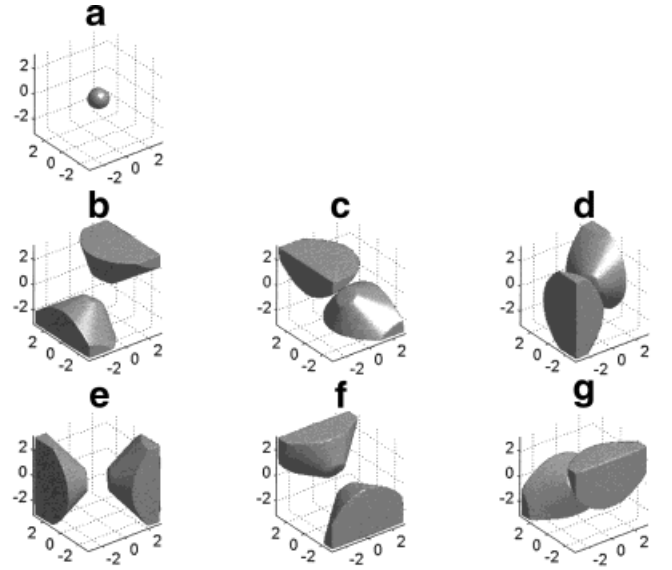


Figure 1. Filter shapes in the Fourier domain. Isosurface plots of the low-pass filter (a) and six directed high-pass filters (b–g) used in the adaptive filtering process. The contribution from each of these filters is controlled by the information from the estimated orientation tensor.

$$\beta_k(\mathbf{x}) = \hat{\mathbf{T}}(\mathbf{x}) \cdot \frac{5}{4} \left(\hat{\mathbf{n}}_k \hat{\mathbf{n}}_k^T - \frac{1}{5} \mathbf{I} \right) \quad (12)$$

and where \cdot defines tensor inner product. The value of α is determined from the norm of the orientation tensor T_{LP} , mapped by a smooth transfer function, $h(\|T_{\text{LP}}\|/\|T_{\text{LP}}\|_{\text{Max}})$, as shown in Figure 2. The threshold level is determined manually from the norm values. A high tensor norm implies a well-defined structure, increasing the contribution from the high-pass filter in that region. Allowing alpha to be higher than 1 makes it possible to increase the high-frequency content in the filtered image. This is useful when a higher image contrast is desired, since the signal intensity close to the edges is increased.

The amount of anisotropy in the high-pass filtering is determined from the normalized orientation tensor \hat{T}_{LP} , which is calculated by dividing T_{LP} by its largest eigenvalue. One large eigenvalue implies a well-defined planar structure, while a line is characterized by two large eigenvalues. The low-pass filter and the six high-pass filters are linearly combined to produce filters that enhance structures like planes or lines (see Fig. 3), or any combination thereof. In this way the filter is composed so that the high-pass filtering is performed only across the structures, with low-pass filtering in the other directions.

Implementation

All calculations were performed in the Fourier domain in order to simplify rescaling of the filters. The filter parameters were specified using a unit volume element having 1 mm/voxel of resolution in the spatial domain. The filter parameters in the Fourier domain were defined in radians in the interval $-\pi$ to $+\pi$ within the unit

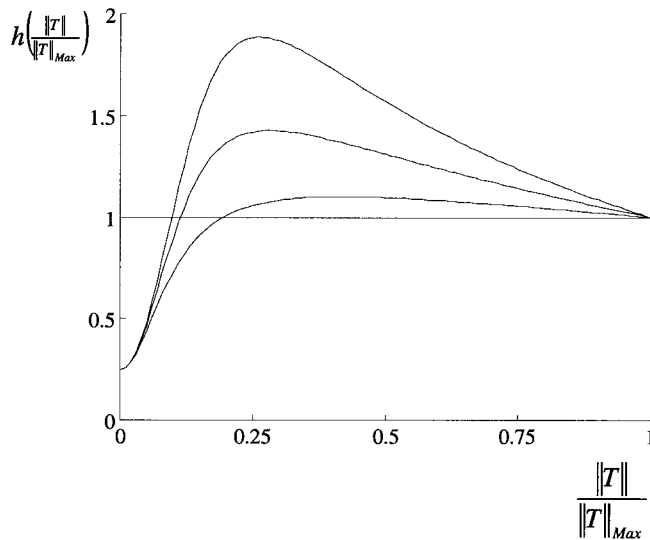


Figure 2. The amount of high-pass filtering (both isotrop and anisotrop) is controlled by the norm of the stabilized filtered orientation tensor, T_{LP} , filtered by a smooth transfer function, $h(\|T_{LP}\|/\|T_{LPMax}\|)$. The different curves represent different amounts of amplification of the high-frequency content in areas where a well-defined structure has been found. Having the transfer function starting at a nonzero value means that a certain amount of high-frequency content is added where no structure is found.

volume. Scaling of the filters was then performed according to the actual resolution. For example, if the resolution of a filtered volume is increased by a factor of 2 in one direction, the corresponding filter bandwidth is reduced to one half.

CNR

CNR estimated on the projection images were studied to evaluate the performance of the implemented method. The definition of CNR proposed by Brown and Riederer (32) is used in this study:

$$\text{CNR} = \frac{s_a - s_b}{\sqrt{\frac{n_a}{n_a + n_b} \sigma_a^2 + \frac{n_b}{n_a + n_b} \sigma_b^2}} \quad (13)$$

where s_a and s_b denote the image intensity in a vessel and the surrounding background, respectively. σ_a^2 and σ_b^2 are the variance of the image intensity in the same areas. n_a and n_b correspond to the number of pixels in the two regions. Areas defined as vessel and background were selected in the MIP images by using a threshold applied to the filtered image and using the result as a mask for both original and filtered data.

MATERIALS AND METHODS

The multidimensional adaptive filtering algorithm was implemented on a SUN Ultra 80 workstation (SUN Microsystems Inc., Mountain View, CA). The program is implemented in C code and consists of several modules, each performing different tasks, such as the estimation

of local structure, relaxation, normalization of the orientation tensor, and the final adaptive filtering. The method was evaluated on a mathematical vessel model and in vivo 3D MRA data. The size of the data sets are $256 \times 256 \times 64$; approximately 3 minutes of CPU time was required for the complete filtering procedure.

A computer-generated vessel phantom was developed consisting of three vessels with diameters of 5, 10, and 15 voxels, respectively (see Fig. 4). Each vessel was created with three different stenoses, giving area reductions of 70%, 80%, and 90% of the original vessel area. Gaussian distributed noise was added, with a variance of 30% of the signal in the simulated vessels (see Fig. 4). Note that the CNR in the maximum projection (MIP) image is higher than in the original 3D volume, due to the nonlinear projection process (29). Simulated phantom images corresponding to image data acquired using repeated scans were constructed (NEX = 1, 2, and 4) by averaging images with independent Gaussian noise.

In vivo data were acquired on a 1.5 T Signa Horizon MRI scanner (GE Medical Systems, Milwaukee, WI), using conventional 3D phase-contrast and 2D TOF pulse sequences. Phase-contrast angiograms of the cerebral vessels were acquired using the head coil and the following scan parameters: TR = 21 msec, TE = 8 msec, flip angle = 30° , field of view (FOV) = 240 mm, slice thickness = 1.5 mm, flow encoding range (V_{enc}) = 30 cm/second. The angiogram of the renal arteries was acquired using the same parameters, but utilizing a rectangular surface coil positioned to cover the right renal branch and a velocity encoding range of 50 cm/second. For the TOF image data, the following scan parameters were used: TR = 45 msec, TE = 4.9 msec, flip angle = 60° , FOV = 200 mm, slice thickness = 1.5 mm.

RESULTS

To verify that the filtering process does not introduce any artifactual structures or alter the assessment of existing stenoses, data from the mathematical vessel phantom were used. MIPs of the image data before and after adaptive filtering are shown in Figures 4b and g and 4e and j, respectively. The shapes of different simulated stenoses are preserved, while the noise level is dramatically reduced. A comparison with noise reduc-

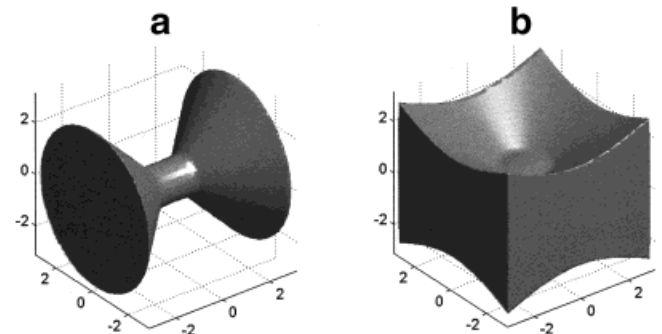


Figure 3. Filter shapes in the Fourier domain. Isosurface plots of two filters composed to enhance planes (a) and lines (b).

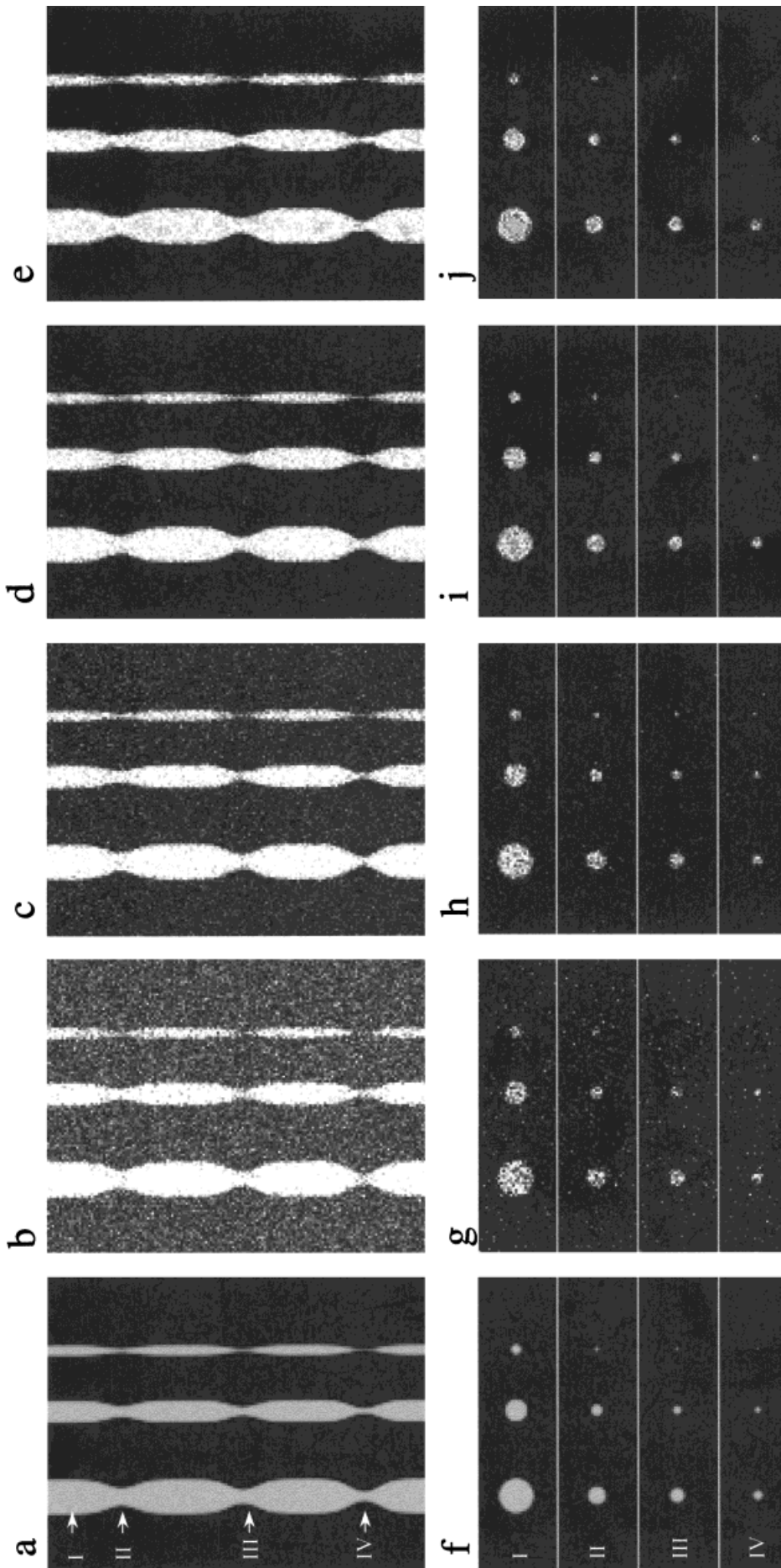


Figure 4. MIPs of data from the vessel phantom. **a:** Original with Gaussian noise added. Images **b**, **c**, and **d** correspond to different numbers of averaged acquisitions, NEX = 1, 2, and 4, respectively. The result of adaptive filtering of the 1 NEX volume data is shown in **e**. Panels **f-j** are showing slices through the 3D data sets, with levels I-IV corresponding to the arrows in **a**. Note that the image quality in the filtered image (**e-j**) is comparable to the 4 NEX data (**d,i**).

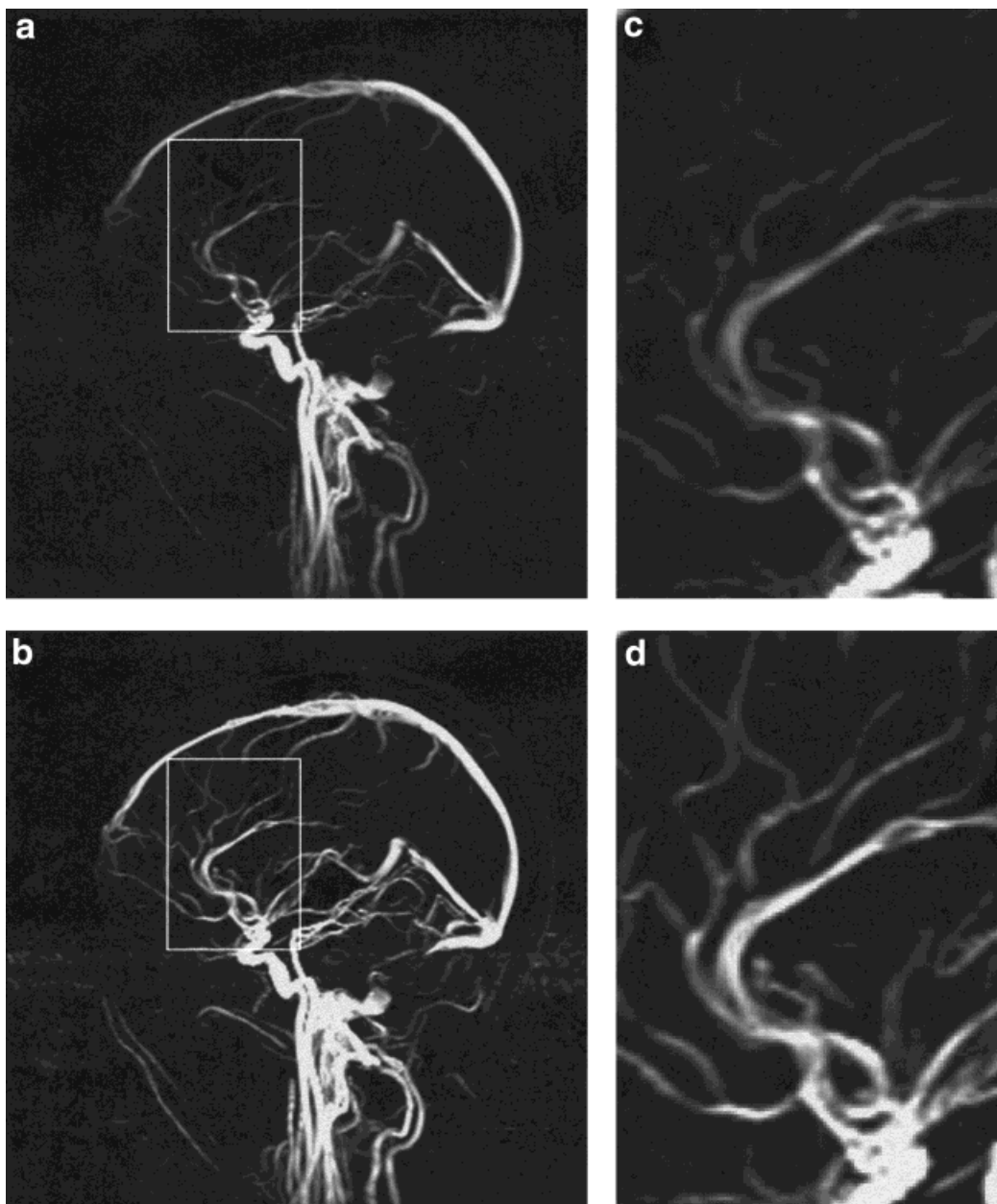


Figure 5. MIPs created from a sagittal 3D phase-contrast data set depicting parts of the cerebral vascular tree. The original data set (**a,c**), and the result after adaptive filtering (**b,d**) are shown. The closeup of the images demonstrates a better delineation of vascular structures and suppression of background noise (**c,d**).

tion using signal averaging of repeated scans is also presented in Figure 4. The estimated CNR in the MIP images for NEX = 1, 2, and 4 were 5.4, 8.0, and 12.0, respectively. The result after adaptive filtering of image data corresponding to 1 NEX gave a CNR of 14.1, i.e., a 162% (8.3 dB) improvement.

A reduction of the noise level can also be seen for the phase-contrast angiogram of the cerebral vessels ($\text{CNR}_{\text{Original}} = 4.6$, $\text{CNR}_{\text{Filtered}} = 7.1$, improvement = 54% (3.8 dB)). In the magnified part of the image (Fig. 5c and d), it is evident that all small structures are preserved and made more visible. The vessels are smoothed along their axial directions and sharpened in their cross-sections. The vessel wall of large vessels will be considered as a planar structure, and smoothing will be performed

accordingly in all directions of this surface, while sharpening is performed across the lumen. The result of adaptive filtering of the 3D phase-contrast data set covering the right renal artery is shown in Figure 6. The peripheral vessels are better delineated, and the overall noise is significantly reduced in the filtered image ($\text{CNR}_{\text{Original}} = 6.1$, $\text{CNR}_{\text{Filtered}} = 17.0$, improvement = 179% (8.9 dB)). Interestingly, the left branch is observable in the filtered axial projection but not in the projection from the original data set. This suggests that the method has the ability to enhance structures obscured by noise.

As expected, stationary tissue is not suppressed as well in the TOF data as in the phase-contrast angiograms (Fig. 7). This is still true in the filtered images,

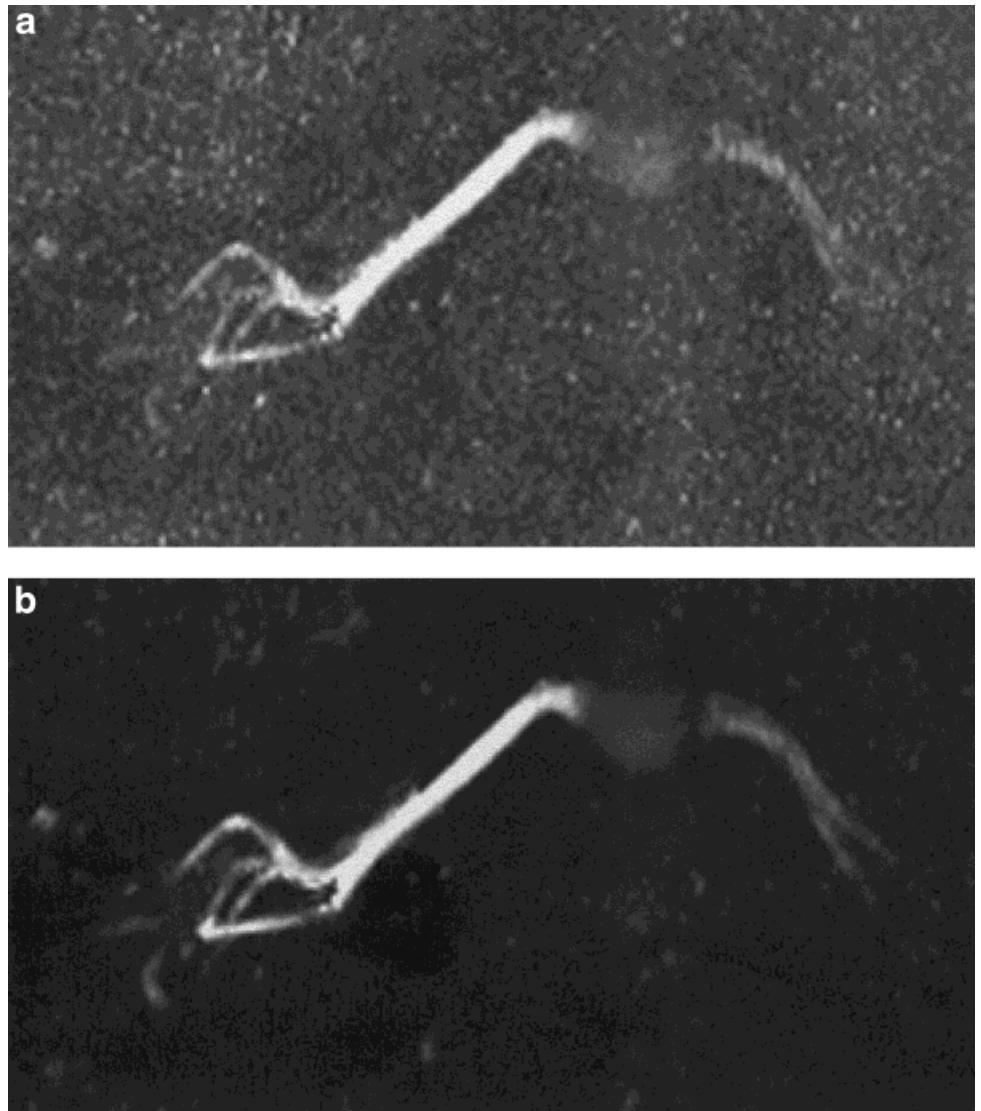


Figure 6. Axial MIP of the original 3D phase-contrast data set covering the right renal artery (a) and the result after the adaptive filtering process (b).

but the noise levels within both vessels and background are markedly reduced images ($CNR_{\text{Original}} = 4.8$, $CNR_{\text{Filtered}} = 6.0$, improvement = 25% (1.9 dB)). Here, the effect of a transfer function, h , with values above 1 is evident in regions with a well-defined structure. The intensity along the vessels is increased, while at the same time low-pass filtering reduces the noise level in other areas.

DISCUSSION

The technique presented here shows promise for improving 3D phase-contrast MRA data. Smaller blood vessels were better delineated at the same time that the high-frequency noise was efficiently suppressed. Structures hidden in the noise could be enhanced using 3D adaptive filtering. Therefore, this method may provide a way to reduce MRA scan time, without losing important diagnostic information.

A limitation of the present implementation is that artifacts present in the original data are not suppressed. If these artifacts have an apparent structure similar to a plane or line, they will be enhanced as well.

This is the case with pulsation or motion artifacts, both of which create ghost artifacts along the phase-encoding direction. This can be seen in Figure 5, where pulsation artifacts in the arteries are more visible in the filtered than in the original data set.

In the present study no optimization of the quadrature filter parameters was performed. The center frequency and the bandwidth of the log normal function were taken from a previous study (20). Further improvements of the CNR and image quality may be achievable by optimizing the filter parameters for MRA data. The possibilities of employing sparse/uncertain field filtering awaits investigation (33,34). In addition, multidimensional filtering is not limited to 3D, and in the future this method will be extended to 4D volume MRI data with temporal resolution (35). The 3D adaptive filtering technique as presented is currently being evaluated on a broader cross-section of clinical material.

APPENDIX A

The directions of the six filters expressed in the tensor notation are given by:

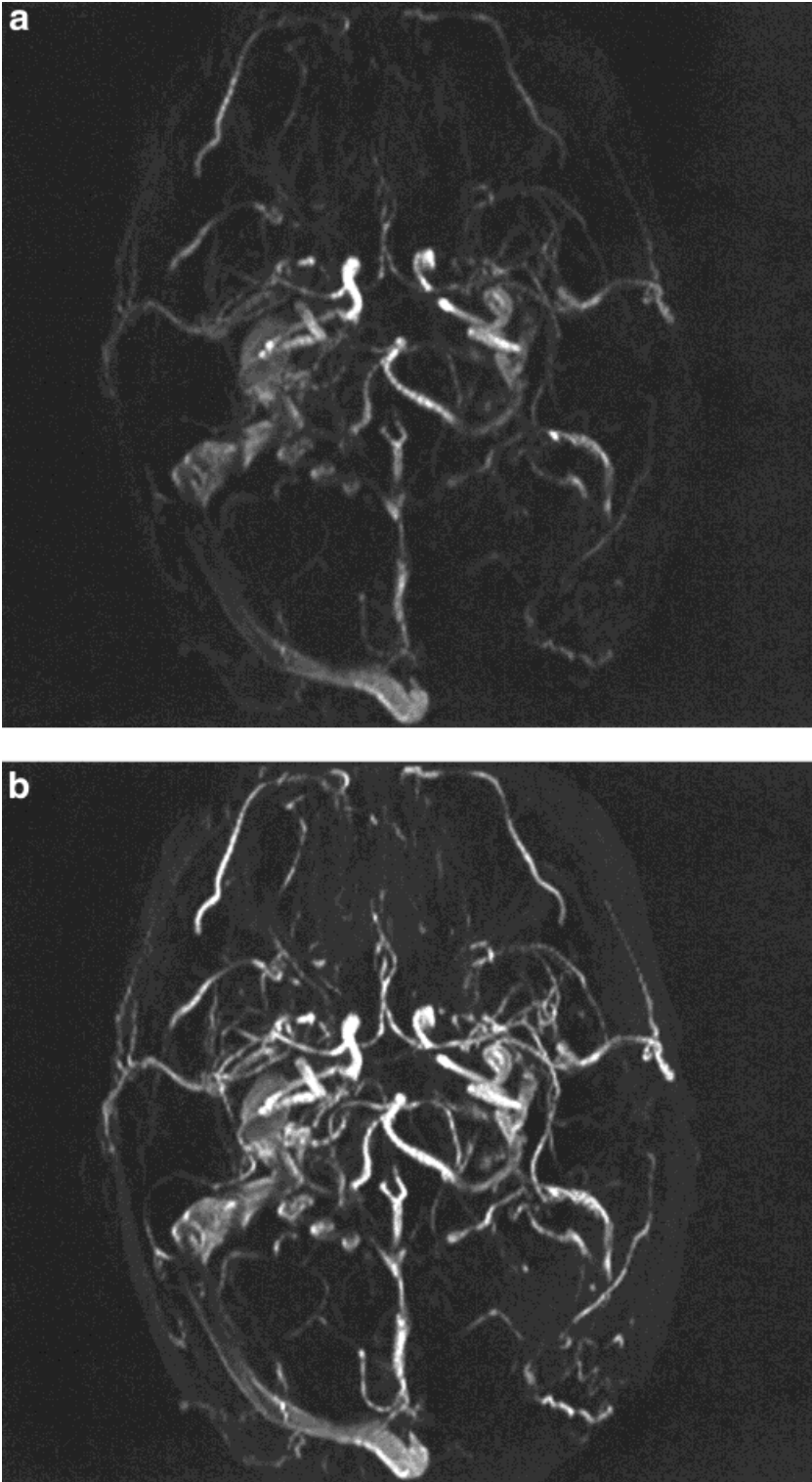


Figure 7. MIPs of TOF MRA data before (a) and after (b) adaptive filtering.

$$N_k = \hat{n}_k \hat{n}_k^t \quad (\text{A.1})$$

$$\hat{n}_5 = c(0 \ b \ a)^T \quad \hat{n}_6 = c(0 \ b \ -a)^T \quad (\text{A.2})$$

where

and

$$\begin{aligned} \hat{n}_1 &= c(a \ 0 \ b)^T & \hat{n}_2 &= c(-a \ 0 \ b)^T \\ \hat{n}_3 &= c(b \ a \ 0)^T & \hat{n}_4 &= c(b \ -a \ 0)^T \end{aligned}$$

$$a = 2 \quad b = 1 + \sqrt{5} \quad c = \frac{1}{\sqrt{10 + 2\sqrt{5}}} \quad (\text{A.3})$$

These six directions are directed toward vertices of a hemi-icosahedron.

REFERENCES

- Dumoulin CL, Souza SP, Walker MF, Wagle W. Three-dimensional phase contrast MR angiography. *Magn Reson Med* 1989;9:139-149.
- Talagala SL, Jungreis CA, Kanal E, Meyers SP, Foo TK, Rubin RA, Applegate GR. Fast three-dimensional time-of-flight MR angiography of the intra-cranial vasculature. *J Magn Reson Imaging* 1995; 5:317-323.
- Laub G. Displays for MR angiography. *Magn Reson Med* 1990;14: 222-229.
- Cline HE, Dumoulin CL, Lorensen WE, Souze SP, Adams WJ. Volume rendering and connectivity algorithms for MR angiography. *Magn Reson Med* 1991;18:384-394.
- Wang Y, Weber DM, Korosec FR, Mistretta CA, Grist CA, Swan JS, Turski PA. Generalized matched filtering for time-resolved MR angiography of pulsative flow. *Magn Reson Med* 1993;30:600-608.
- Caprihan A, Igenogle MV. A weighted least-squares method for nuclear magnetic resonance velocity imaging. *Magn Reson Med* 1993;29:512-520.
- Itagaki H. Improvements of nuclear magnetic resonance image quality using iterations of nonlinear filtering. *IEEE Trans Med Imaging* 1993;12:322-327.
- Soltanian-Zadeh H, Windham JP, Peck DJ, Yagle AE. A comparative analysis of several transformations for enhancement and segmentation of magnetic resonance image scene sequences. *IEEE Trans Med Imaging* 1992;11:302-318.
- Soltanian-Zadeh H, Windham JP. Mathematical basis of eigenimage filtering. *Magn Reson Med* 1994;31:465-466.
- Song SM, Napel S, Glover GH, Pelc NJ. Noise reduction in three-dimensional phase-contrast MR velocity measurements. *J Magn Reson Imaging* 1993;3:587-596.
- Du YP, Parker DL, Davis WL. Vessel enhancement filtering in three-dimensional MR angiography. *J Magn Reson Imaging* 1995;5:353-359.
- Perona P, Malik J. Scale space and edge detection using anisotropic diffusion. *IEEE Trans Pattern Anal Machine Intel* 1990;12:629-639.
- Gerig G, Kubler O, Kikinis R, Jolesz FA. Nonlinear anisotropic filtering of MRI data. *IEEE Trans Med Imaging* 1992;11:221-232.
- Alvarez L, Guichard F, Lions PL, Morel JM. Axioms and fundamental equations of image processing. *Arch Rational Mechanics* 1993; 123:200-257.
- Sapiro G, Tannenbaum A. Affine invariant scale space. *Int J Comp Vision* 1993;11:25-44.
- Chen H, Hale J. An algorithm for MR angiography image enhancement. *Magn Reson Med* 1995;33:534-540.
- Koller TM, Grieg G, Szekeley G, Dettwiler D. Multiscale detection of curvilinear structures in 2D and 3D image data. In: *Proceedings of the International Conference on Computer Vision*, 1995. p 864-869.
- Sun Y, Lucariello RJ, Chiaramida SA. Directional low-pass filtering for improved accuracy and reproducibility of stenosis quantification in coronary arteriograms. *IEEE Trans Med Imaging* 1995; 14:242-248.
- Sato Y, Nakajima S, Shiraga N, Atsumi H, Yoshida S, Koller T, Gerig G, Kikinis R. Three-dimensional multi-scale line filter for segmentation and visualization of curvilinear structures in medical images. *Med Image Anal* 1998;2:143-168.
- Granlund GH, Knutsson H, editors. *Signal processing for computer vision*. Dordrecht: Kluwer Academic Publishers; 1995. p 297-365.
- Knutsson H, Wilson R, Granlund GH. Anisotropic non-stationary image estimation and its applications—part I: restoration of noisy images. *IEEE Trans Comm* 1983;31:388-397.
- Knutsson H, Haglund L, Bärman H, Granlund GH. A framework for anisotropic adaptive filtering and analysis of image sequences and volumes. In: *Proceedings of ICASSP-92, San Francisco, CA, 1992*. IEEE 3:469-472.
- Haglund L. *Adaptive multidimensional filtering*. Linköping studies in science and technology. PhD dissertation 284. Sweden: Linköping University; 1992.
- Westin C-F, Richolt J, Moharir V, Kikinis R. Affine adaptive filtering of CT data. *Med Image Anal* 2000;4:161-177.
- Knutsson H. *Filtering and reconstruction in image processing*. Linköping studies in science and technology. PhD dissertation 88. Sweden: Linköping University; 1982. Chapter 4:1-62.
- Granlund GH. In search of a general picture processing operator. *Comp Graph Imaging Process* 1978;8:155-173.
- Knutsson H. Representing local structure using tensors. In: *Proceedings of the 6th Scandinavian Conference on Image Analysis*. Oulu, Finland, 1989. p 244-251.
- Knutsson H, Bärman H, Haglund L. Robust estimation in 2D, 3D and 4D using tensors. In: *Proceedings of the International Conference on Automation, Robotics and Computer Vision, ICARCV92, Singapore, 1992*. CV-5.4.1-CV-5.4.5.
- Knutsson H. A tensor representation of 3-D structures. In: *Proceedings of the 5th IEEE-ASSP and EURASIP Workshop on Multidimensional Signal Processing*, Noordwijkerhout, 1987.
- Westin C-F, Knutsson H. Estimation of motion vector fields using tensor field filtering. In: *Proc. IEEE Int. Conf. Image Proc. (ICIP)*, Austin, TX, 1994. p 237-242.
- Westin C-F, Bhalerao A, Knutsson H, Kikinis R. Using local 3D structure for segmentation of bone from computer tomography images. In: *Proc. IEEE Conf. Comp. Vision and Pattern Recognition (CVPR)*. Puerto Rico, 1997. p 794-800.
- Brown DG, Riederer SJ. Contrast-to-noise ratios in maximum intensity projection images. *Magn Reson Med* 1992;23:130-137.
- Knutsson H, Westin C-F. Normalized and differential convolution: methods for interpolation and filtering of incomplete and uncertain data. New York City: CVPR, IEEE; 1993. p 515-523.
- Westin C-F. *A tensor framework for multidimensional signal processing*. Linköping studies in science and technology. Dissertation 348. Sweden: Linköping University; 1994.
- Wigström L, Sjöqvist L, Wranne B. Temporally resolved 3D phase-contrast imaging. *Magn Reson Med* 1996;36:800-803.